Linking fracture networks to geophysical observations through numerical modelling

Alison Kirkby[1]

[1]GNS Science, Wairakei Research Center, 114 Karetoto Road, Taupo 3384, New Zealand

a.kirkby@gns.cri.nz

Keywords: *Permeability, resistivity, numerical model, fractures*

ABSTRACT

Fractures are often a key control on geothermal reservoir permeability. Knowing their orientation can help design wells with the best chance of intersecting them. Borehole image log analysis can provide this information but relies on boreholes being drilled first and provides information only in a small region around the borehole. Electrical resistivity and acoustic velocity are both direction-dependent properties that may be sensitive to the orientation of subsurface features at wider scales and without the need for drilling. Shear wave splitting has been applied in some New Zealand geothermal fields and may provide an estimate of fracture orientation but is not directly sensitive to permeability. Electrical resistivity of a rock can vary with orientation, and the electrical resistivity of a reservoir containing aligned open fractures with a preferred orientation may be resolved by geophysical methods as effective anisotropy. However, most subsurface resistivity models assume isotropic resistivity. Geothermal fields in the Taupō Volcanic Zone (TVZ), New Zealand, have been developed for electricity for >50 years and as such, the TVZ contains a wealth of scientific publications from which to define fracture parameters and fluid properties. This paper presents numerical modelling of the permeability and resistivity of a fractured rock volume containing a fluid with typical salinity and temperature for TVZ fields, to determine effective (direction-dependent) resistivity and permeability, and ground truth the models by comparing with permeability values calibrated from reservoir models. This is the first step to designing a geophysical survey that could image fracture orientation.

1. INTRODUCTION

The nature and orientation of open structures is a key consideration in understanding a geothermal reservoir and designing productive wells. However, this information is not normally available until several wells have been drilled and borehole image analysis has been completed to characterize in situ structures and stress field.

Both resistivity and acoustic rock properties can be anisotropic, i.e. they vary with orientation, which provides an opportunity to measure the direction-dependent resistivity and/or velocity of fractured rock and relate this to permeability. Borehole image analysis makes use of both properties (e.g. McNamara et al. 2015, Massiot et al. 2017, McNamara et al. 2019, Milicich et al. 2023). Resistivity-based geophysical techniques such as the magnetotelluric method have been applied widely in geothermal fields across the world, as they are sensitive to several features of interest in a geothermal system: conductive clay alteration zones that commonly overly the upflow zone of a high temperature geothermal field (e.g. Ussher et al. 2000, Cumming and Mackie 2010, Ardid et al. 2021), hot fluids (e.g. Ishizu et al. 2022, Yamaya et al. 2022), and heat sources (e.g. Bertrand et al. 2022). However, these models typically assume resistivity isotropy to reduce the number of parameters to be solved. Shear wave splitting has shown promise in characterizing fractures in several geothermal fields (Elkibbi and Rial 2005, Mroczek et al. 2020, Jylhänkangas 2024), and may provide complementary information to resistivity models.

If a directional dependence of either of these properties is measurable, and its orientation is resolvable, this may provide opportunities for knowing open fracture orientations at an earlier stage of development than is currently possible, leading to improved success in developing a reservoir.

The first step in understanding what attributes of a subsurface fracture network are measurable is to improve understanding of petrophysical properties of fracture networks on a reservoir scale. This could eventually lead to the ability to design geophysical surveys to measure these attributes, and a closer link between geophysical models and reservoir models. The work presented here aims to use numerical fracture models, building on earlier work (Kirkby et al 2016, 2017), to understand the effect that open and aligned fractures have on both permeability and resistivity of a high-temperature geothermal reservoir.

2. METHODS

This work builds on previous work modelling the permeability and resistivity of both individual fractures (Kirkby et al. 2016) and fracture networks (Kirkby and Heinson 2017). This previous work was limited in scale to up to 10 x 10 cm fractures or 1.5 x 1.5 x 1.5 cm cubes, to allow accurate modelling of sub-mm scale roughness on faults. To address the problem of scale, the approach presented here is a multi-2D approach (Figure 1).

Step (1): The permeability and resistivity of different sized fractures is characterized following the approach of Kirkby et al. (2016). This approach is implemented in Python and models resistivity using Ohm's Law, and permeability using a modified local parallel plate model, with locally variable aperture within the fracture. Fluid flow is modelled perpendicular to the slip direction of the fracture, with no flow boundary conditions on the sides of the fracture, and constant pressure/voltage boundary conditions on each end. The resulting fault resistivity is defined, for the purposes of further modelling, as the equivalent resistivity of a hypothetical, uniformly thick sheet that could replace the actual fracture. The sheet has a constant width equal to the mean aperture of the fracture, and its resistivity is computed such that it preserves the same overall electrical response as the original fracture. Defining fracture resistivity in this way allows the fracture resistivity to be easily up-scaled to a desired width, e.g. the bulk resistivity over a width of 1 cm, or desired cell-size in a larger model.

ISSN 2703-4275

Step (2): a 'fault-stick' network is built, like the approach of Kissling and Massiot (2023) except that flow and current is permitted within the matrix as well as within fractures. Permeability and resistivity are modelled along two orthogonal directions, allowing an estimate of the anisotropy in permeability and resistivity. Fault permeabilities and resistivities from step (1) are transferred to the fault stick models, which then provide estimates of hydraulic and electrical properties that are likely to be observed at the scale of a geothermal reservoir. To accommodate different scales, step (2) is split into two steps to characterize the effects of fractures on different length scales. These scales are termed "micro" and "macro" scales, split according to a threshold of 0.1 m in length. First, a 1m x 1m fault area containing fractures ≤0.1 m in size is modelled. The bulk permeability and resistivity values calculated from these models are then used as matrix permeabilities and resistivities for a larger fault volume, 16 x 16 m.

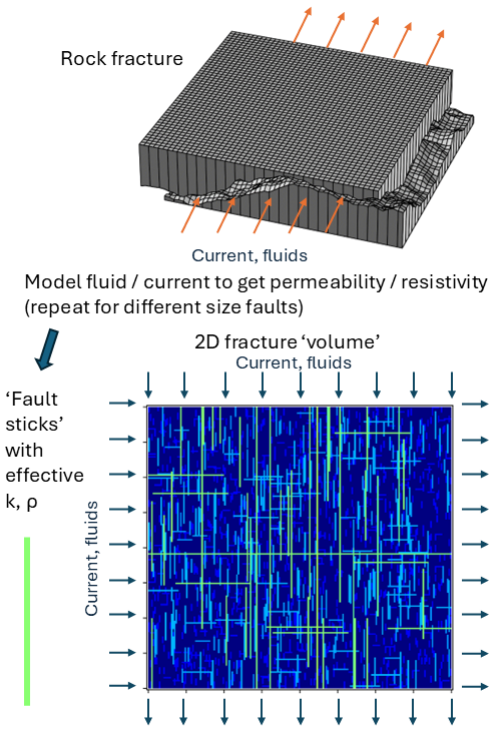

Figure 1. Diagram illustrating methodology used to model fractured reservoir properties. The top panel describes modelling of fracture properties, to determine effective properties of individual fractures. In the bottom panel, the combined effect of many fractures, each with effective resistivity and permeability (determined from the top panel) is modelled to get the resistivity and permeability of a fractured volume. In the diagram, k=permeability and ρ=resistivity.

There are several parameters that need to be defined to build individual fault models and fracture network models. For individual fault models, parameters include size, fractal dimension and scaling factor for fault surface height amplitude, which influence the roughness of fracture planes (Matsuki et al. 2006, Kirkby et al. 2016), fault displacement (which broadly scales with fault size (Kim and Sanderson 2005)), fluid resistivity, matrix resistivity and permeability. Parameters used in this paper are summarized in Table 1. The fault stick models are constructed using a power law fault length distribution defined by:

$$N_f = \frac{\alpha}{1-a} l_{min}^{1-a} R^2 \quad \text{(Bonnet et al. 2001)}$$

Where N_f is the number of faults of length greater than l_{min}, R^2 is the area in which these faults occur, and α and a are respectively the density constant and density exponent of the power law distribution. Instead of defining α, target fracture porosity was defined, then the α value needed to give that target fracture porosity was calculated. For the models presented here, a was set to 2.7 with two models run setting fracture porosity of 2.5 and 4.5 % respectively.

A summary of the parameters used in the models shown in this paper are also shown in Table 1.

3. RESULTS

The distribution of resistivity and permeability of individual fractures from modelling is shown in Figure 2 as stacked histograms. Broadly, permeability increases with fault length, reflecting the increased aperture size that is generated by having increased offset. In contrast, fault resistivity does not vary significantly with length, with a median value of 5 Ωm regardless of the size of the fault. However, the harmonic mean resistivity over the width of a cell in the upscaled model (1 cm) decreases with fault size, reflecting the larger mean fault width.

Table 1. Parameters used in models of fracture permeability and resistivity

Individual fault parameters	
Length	5 mm to 10 m (11 fault lengths total). Faults with length < 5 cm were assumed to have the same properties as 5 cm faults.
Cell size	Length / 500
Displacement	0.02 x length
Fractal dimension	2.3
Scaling factor	0.003
Area of contact between fracture planes	34 to 51 %
Fluid resistivity	0.5 Ωm
Matrix resistivity	1000 Ωm
Matrix permeability	10^{-18} m^2
Number of repeats	96
Fracture network parameters	
Cell size	1 mm (1 m x 1m model) 1 cm (16 m x 16 m model)
Fault density exponent (a)	2.7
Fracture porosity	2.5 and 4.5 %
Percentage of faults striking NE–SW / NW–SE	85 / 15
Number of repeats	100

The mean permeability of the reservoir area from fault stick models is shown in Figure 3, and resistivity in Figure 4. Increasing fracture porosity from 2.5 to 4.5 % causes an increase in fault permeability by about an order of magnitude, and a decrease in resistivity by a factor of about 3 to 6. While fractures ≤ 0.1 m length contribute a relatively small amount to overall permeability (< 1 order of magnitude, compared to 4-5 orders of magnitude change from the larger fractures), they contribute to a greater degree to the resistivity, reducing resistivity by a similar factor as the larger fractures.

In the large scale fracture networks, resistivity anisotropy (i.e. ratio of resistivity across the dominant strike direction of the fracture network to along strike) ranges from a factor of 2.4 to 2.8 and is highest in the high porosity case (4.5 %). Conversely, permeability anisotropy is higher in the low porosity case (median factor of 25) compared to the high porosity case (median factor of 8).

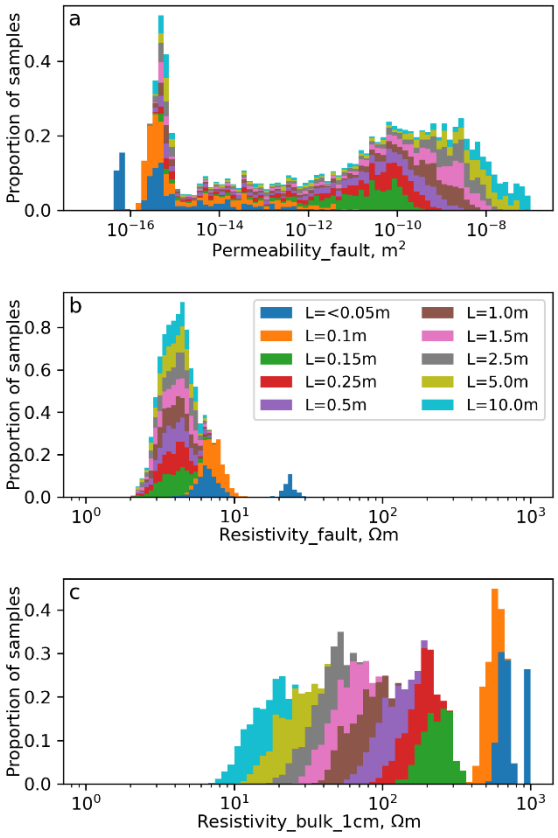

Figure 2. Stacked histograms showing permeabilities and resistivities of fractures from modelling. (a) fault permeability, (b) fault resistivity (see Section 2 for discussion on how this is defined), (c) resistivity averaged over a width of 1 cm (assuming a matrix resistivity of 1000 Ωm).

4. DISCUSSION AND CONCLUSION

Numerical modelling quantifies the hydraulic and electrical properties of a fractured reservoir, based on properties of TVZ geothermal systems. The preliminary models presented in this paper highlight a few key findings:

1. Micro-scale (≤ 0.1 m) fractures contribute relatively little to the overall permeability enhancement but have a more significant effect to bulk resistivity
2. An increase in fracture porosity from 2.5 to 4.5 % is associated with fracture permeability enhancements of about an order of magnitude, and a reduction in resistivity by a factor of 2, along the strike of the fault network; and
3. For the parameters considered here, bulk (large-scale) permeability anisotropy in the fractured reservoir ranges from a factor of 8 to 25 and resistivity anisotropy ranges from a factor of 2.4 to 2.8.

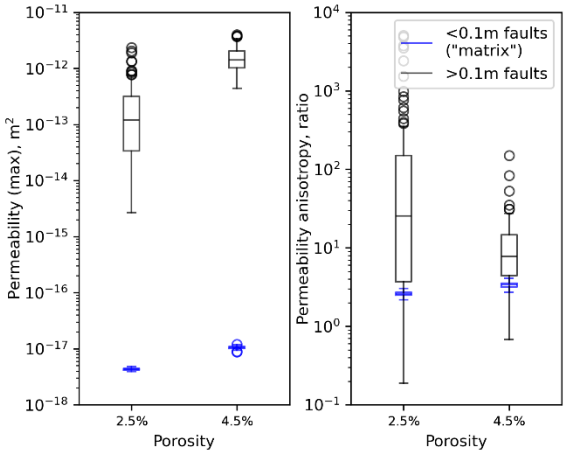

Figure 3. Bulk (<0.1m faults) and fracture (>0.1m faults) permeability (left) and permeability anisotropy (right) in two fractured volume models (2.5 % porosity and 4.5 % porosity). In an extensional regime such as the Taupō Volcanic Zone, the permeability represents along-strike permeability and the anisotropy is along-strike / across-strike permeability.

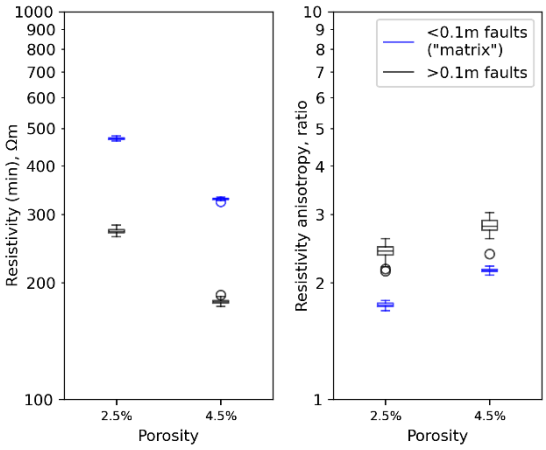

Figure 4. Small-scale (<0.1m faults) and reservoir-scale (including >0.1m faults) resistivity (left) and resistivity anisotropy (right) predicted by fractured reservoir models with total fracture porosity equal to 2.5 and

4.5 %. In an extensional regime such as the Taupō Volcanic Zone, the resistivity represents along-strike resistivity, and the anisotropy is across-strike / along-strike resistivity.

Work is ongoing to explore the sensitivity of the results to different model inputs, including fracture length distribution parameters, total model area, and fluid resistivities. The aim is to work toward understanding theoretical resistivity tensors that can be used to model the sensitivity of different resistivity-based geophysical techniques to fracture orientation, and design surveys or modelling methods that can resolve directional-dependence of resistivity. This may ultimately allow information about fracture orientations to become available at an earlier stage of development than is currently possible.

REFERENCES

Ardid, A., D. Dempsey, E. Bertrand, F. Sepulveda, P. Tarits, F. Solon and R. Archer (2021). "Bayesian magnetotelluric inversion using methylene blue structural priors for imaging shallow conductors in geothermal fields." *Geophysics* **86**(3): E171-E183.

Bertrand, E. A., P. Kannberg, T. G. Caldwell, W. Heise, S. Constable, B. Scott, S. Bannister, G. Kilgour, S. L. Bennie, R. Hart and N. Palmer (2022). "Inferring the magmatic roots of volcano-geothermal systems in the Rotorua Caldera and Okataina Volcanic Centre from magnetotelluric models." *Journal of Volcanology and Geothermal Research* **431**: 107645.

Bonnet, E., O. Bour, N. E. Odling, P. Davy, I. Main, P. Cowie and B. Berkowitz (2001). "Scaling of fracture systems in geological media." *Reviews of Geophysics* **39**(3): 347-383.

Cumming, W. and R. Mackie (2010). Resistivity Imaging of Geothermal Resources Using 1D, 2D and 3D MT Inversion and TDEM Static Shift Correction Illustrated by a Glass Mountain Case History. *Proc World Geothermal Congress 2010*. Bali, Indonesia.

Elkibbi, M. and J. A. Rial (2005). "The Geysers geothermal field: results from shear-wave splitting analysis in a fractured reservoir." *Geophysical Journal International* **162**(3): 1024-1035.

Ishizu, K., Y. Ogawa, K. Nunohara, N. Tsuchiya, M. Ichiki, H. Hase, W. Kanda, S. Sakanaka, Y. Honkura, Y. Hino, K. Seki, K. H. Tseng, Y. Yamaya and T. Mogi (2022). "Estimation of Spatial Distribution and Fluid Fraction of a Potential Supercritical Geothermal Reservoir by Magnetotelluric Data: A Case Study From Yuzawa Geothermal Field, NE Japan." *Journal of Geophysical Research: Solid Earth* **127**(2): e2021JB022911.

Jylhänkangas, S. (2024). Comparing theoretical with measured seismic anisotropy in the Central Taupō Volcanic Zone. MSc, Victoria University of Wellington.

Kim, Y.-S. and D. J. Sanderson (2005). "The relationship between displacement and length of faults: a review." *Earth-Science Reviews* **68**(3): 317-334.

Kirkby, A. and G. Heinson (2017). "Three-dimensional resistor network modeling of the resistivity and permeability of fractured rocks." *Journal of Geophysical Research: Solid Earth* **122**(4): 2653-2669.

Kirkby, A., G. Heinson and L. Krieger (2016). "Relating permeability and electrical resistivity in fractures using random resistor network models." *Journal of Geophysical Research: Solid Earth* **121**(3): 1546-1564.

Kissling, W. M. and C. Massiot (2023). "Modelling of flow through naturally fractured geothermal reservoirs, Taupō Volcanic Zone, New Zealand." *Geothermal Energy* **11**(1): 20.

Massiot, C., A. Nicol, D. D. McNamara and J. Townend (2017). "Evidence for tectonic, lithologic, and thermal controls on fracture system geometries in an andesitic high-temperature geothermal field." *Journal of Geophysical Research: Solid Earth* **122**(8): 6853-6874.

Matsuki, K., Y. Chida, K. Sakaguchi and P. W. J. Glover (2006). "Size effect on aperture and permeability of a fracture as estimated in large synthetic fractures." *International Journal of Rock Mechanics and Mining Sciences* **43**(5): 726-755.

McNamara, D. D., C. Massiot, B. Lewis and I. C. Wallis (2015). "Heterogeneity of structure and stress in the Rotokawa Geothermal Field, New Zealand." *Journal of Geophysical Research: Solid Earth* **120**(2): 1243-1262.

McNamara, D. D., S. D. Milicich, C. Massiot, P. Villamor, K. McLean, F. Sépulveda and W. F. Ries (2019). "Tectonic Controls on Taupo Volcanic Zone Geothermal Expression: Insights From Te Mihi, Wairakei Geothermal Field." *Tectonics* **38**(8): 3011-3033.

Milicich, S. D., C. Massiot and B. Murphy (2023). Fracture permeability in basement greywacke for supercritical drilling planning. *Proc. 45th New Zealand Geothermal Workshop*, Auckland, New Zealand.

Mroczek, S., M. K. Savage, C. Hopp and S. M. Sewell (2020). "Anisotropy as an indicator for reservoir changes: example from the Rotokawa and Ngatamariki geothermal fields, New Zealand." *Geophysical Journal International* **220**(1): 1-17.

Ussher, G., C. Harvey, R. Johnstone and E. Anderson (2000). Understanding the Resistivities Observed in Geothermal Systems. *Proc. World Geothermal Congress 2000*, Kyushu - Tohoku, Japan.

Yamaya, Y., Y. Suzuki, Y. Murata, K. Okamoto, N. Watanabe, H. Asanuma, H. Hase, Y. Ogawa, T. Mogi, K. Ishizu and T. Uchida (2022). "3-D resistivity imaging of the supercritical geothermal system in the Sengan geothermal region, NE Japan." *Geothermics* **103**: 102412.

ISSN 2703-4275